

The ERS Scatterometer instrument and the On-Ground processing of its Data.

Pascal Lecomte

Directorate of Application Programmes - Remote Sensing Exploitation Division
ERS Mission Control and Product Assurance Section
ESA / ESRIN, Via Galileo Galilei, 00044 Frascati, Italy
tel: ++39-6-941 80 670, fax: ++39-6-941 80 612
Email: pascal.lecomte@esrin.esa.it

Introduction

The ERS scatterometer is a radar working at 5.3 GHz (C-Band) designed to measure the wind speed and direction. This instrument has three antennae looking 45° forward, sideways and 45° backwards with respect to the satellite's flight direction.

The radar is sensitive to the sea surface roughness which is directly related to the wind characteristics (speed and direction) near to the surface. Measuring the surface roughness, one can derive information on the wind.

More recently it has been found that scatterometer data are also very valuable for land, snow and ice applications. Parameters like surface moisture, sea ice concentrations, sea ice age and snow conditions could be successfully retrieved using scatterometer data. Particularly promising is the derivation of sea ice masks based on the polarization ratios of the scatterometer data (for NSCAT) and on the different backscatter level behaviour at different incidence angles (for ERS scatterometer), which compare well to similar products derived from SSM/I data. Over land, studies are showing the usefulness of scatterometer data to determine the impact of a lack of rain fall in sahelian areas and can help in having an early drought warning in these regions.

The scope of this document is to describe in detail the characteristics of the Scatterometer raw data when received by the ground station and of the various algorithms used during the generation of the sigma nought and of the wind products.

The ERS Satellites

On 17 July 1991 the European Space Agency launched ERS-1 into a sun-synchronous, polar orbit at an altitude of about 780 km and an inclination of 98.5°, followed by ERS-2 launched in April 1995.

ERS-1 is an Earth Observation satellite that observes the ocean, the sea ice, the cryosphere and the land surface. The satellite (Fig. 1) carries three active microwave instruments: a synthetic aperture radar (SAR), a wind scatterometer, and a radar altimeter (RA) and an infra-

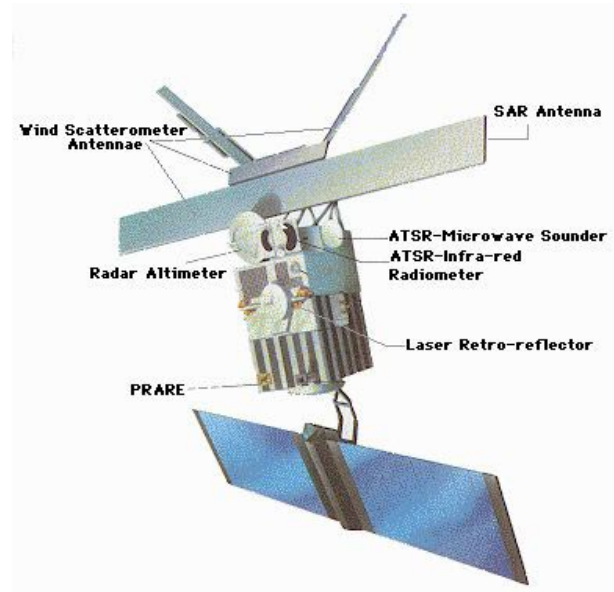


Figure 1: The ERS-1 satellite

red-visible Along Track Scanning Radiometer (ATSR) and a MicroWave Radiometer, mainly dedicated to the retrieval of atmospheric corrections for the RA. The RA and ATSR instruments collect data continuously while the Active Microwave Instrument (AMI) containing the SAR and the wind scatterometer are configured in an alternating operation so that the SAR Wave Mode runs jointly with the wind scatterometer while the SAR Image Mode only runs with the scatterometer turned off [1].

Both ERS-1 and ERS-2 satellites have a standard orbit repeat cycle of 35 days. Two other repeat cycles of 3 days and 168 days have also been operated with ERS-1.

The Active Microwave Instrument

AMI Main Characteristics

The AMI is a radar operating at 5.6 cm wavelength at a frequency of 5.3 GHz (C-Band). It has a set of four different antennae to illuminate the Earth's surface and to receive backscattered energy. By on-board and on-ground signal processing, two-dimensional imagery is produced. In the picture elements the intensities represent the normalised radar backscattering coefficients (σ^0)

and x and y coordinates correspond to the along-track and cross-track position of the areas being observed. It is identical on both ERS-1 and ERS-2 satellites.

Areas of interest for observation include the polar ice caps, the ocean, coastal zones and the land areas. The realisation of the mission objectives for the AMI, as specified in geophysical terms, rely on the fact that the radar backscattering is affected by surface roughness, conductivity and dielectric properties of the area under observation. Consequently, surface properties can be derived from radar imagery. In the framework of the ERS mission the surface wind speed, wind direction and wave image spectra are routinely estimated from radar data in near real-time. For other applications, the radar imagery is the primary output product.

In addition to surface properties, isolated point targets (ships, icebergs, buildings, etc.) show up in the radar imagery as bright spots as long as their radar cross sections are big enough. The controlling factor is the ratio of the radar cross section of the point target to the product of the normalised radar cross section (σ^0) of the surrounding area and the radar resolution cell.

AMI Functional Description

To meet the geophysical mission objectives, the AMI has to provide imagery with different characteristics to match each application. It, therefore, has three modes of operation, namely the Image Mode, the Wave Mode and the Wind Mode.

For this, two separate radars are incorporated within the AMI. A Synthetic Aperture Radar (SAR) provides the Images and the Wave Modes of operation and a Scatterometer provides the Wind Mode operation. The operational requirements are such that each mode should function independently. However, in addition, the Wind and Wave Modes are capable of interleaved operation, i.e. the so-called Wind/Wave Mode.

The AMI functional block diagram is shown in Fig. 2.

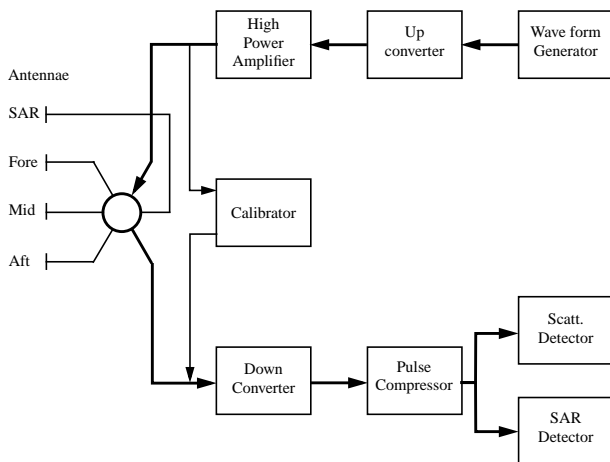


Figure 2: Active Microwave Instrument Block Diagram

The Wind Mode

The measurement objective of this mode is the determination of wind speed and direction over the ocean. Its geophysical performance is specified in Table 3.

Table 1: Scatterometer Geophysical Specifications

Swath width	500 km
Spatial resolution	50 km
Grid Spacing	25 km
Wind speed: accuracy:	0.5 to 30 m/s (s.d.) 2 m/s (bias) 0.3 m/s
Wind direction accuracy	0 to 360 ° (s.d.) 20 ° (bias) 0.8 °

The principle underlying the operation of the scatterometer is the dependence of normalised radar cross section on ocean roughness, which in turn is dependent upon the surface wind speed. In addition, the normalised radar cross section is anisotropic with respect to the angle between wind vector and incident radar beam.

The wind scatterometer is configured as a real aperture pulse radar providing three radar images of the ocean surface with a spatial resolution of 50 km and a swath width of 500 km. The three images are acquired by three different antennas: one, the mid-beam, looking to the right side of the satellite, perpendicular to the ERS ground track, one looking forward at 45 degrees azimuth projection angle, with respect to the mid-beam, and one looking backwards at 45 degrees azimuth projection angle with respect to the mid-beam, as depicted in the scatterometer radar geometry in Fig. 1.

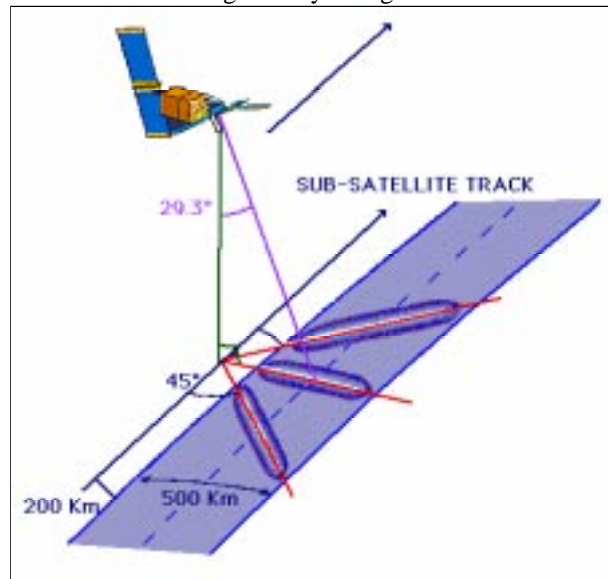


Figure 3: The ERS satellite scatterometer geometry

With the aid of these three σ^0 measurements of the same area made from different measurement directions,

wind vectors (speed and direction) can be determined. The conversion of σ^0 values into wind data is performed for each node with the aid of mathematical model, CMOD4 [2], which defines the relationship between σ^0 , wind speed and wind direction, incidence angle of the scatterometer pulse and polarisation.

The scatterometer illuminates the sea surface sequentially by RF pulses in different directions using the three antennae. The nominal look angles of these antennae are 45° fore and aft and broadside with respect to the satellite's velocity vector. This model is based on the pre-launch estimate of the radar backscattering behaviour, which was determined during a multi-year programme of experiments, using airborne radars, but 'tuned' in orbit on the basis of dedicated geophysical validation campaigns and data assimilation into numerical weather prediction models.

Radar echo is provided continuously over a 500 km wide continuous swath along the satellite ground track so wind speed and direction can be deduced at nodes which have a 25 km separation along and across the sun-satellite track within the swath.

Each node is centered within a resolution cell of 50 x 50 km², which is determined in the range and direction by appropriate range gating of the received echo signal and in azimuth by the averaging of corresponding range-gated echo signals.

In order to achieve the correct illumination of these nodes by all three beams and to minimise Doppler shifts, the satellite is steered about its yaw axis such that the effects of Earth rotation is counteracted.

In Wind Mode, the transmit pulse is produced at the intermediate frequency by the platform generator. The IF pulse is amplified and converted to an RF signal in the up-converter unit and amplified by the High-Power Amplifier. The transmit signal is routed to the correct antenna by the circulator assembly, which in this mode is under the control of the scatterometer electronic unit.

The received signal is down-converted, amplified and routed to the scatterometer detector.

Vital to many applications of scatterometer data is absolute calibration, defined as the process by which the digital output of the instrument is converted into physical units of radar cross-section per unit area, sigma nought, with known levels of accuracy and precision. Therefore noise measurements and internal calibration are regularly performed.

For the Mid Antenna, the return echo if filtered and sampled in complex form (i.e. I and Q). Since the Doppler variation is significant over the swath width (20 kHz near swath to 140 kHz far swath from the Side antennae), a programmable Doppler compensation law is applied on the receiver signal before filtering and complex sampling.

The main engineering parameters of the AMI wind scatterometer mode are given in Table 3.

Table 2: AMI Wind mode Main Engineering Parameters

Frequency	5.3 GHz 52 kHz		
Polarisation	Linear Vertical		
Swath	500 km		
Peak Power (RF)	4.8 kW		
	Fore	Mid	Aft
Antenna aspect angle	+45° 0.5°	0° 0.5°	-45° 0.5°
Antenna length	3.6 m	2.5 m	3.6 m
Dynamic range	42 dB		
Pulse length	130 s	70 s	130 s
No. of pulses per 50 km	256	256	256
Radiometric resolution (Kpe)	6 %	6 %	6 %
Detection Bandwidth	25 kHz	25 kHz	25 kHz
Sampling Scheme	Complex I/Q 8 bits each		
Return Echo window duration	3.93 ms	2.46 ms	3.93 ms

Operational Constraints

The AMI image mode can be operated for up to 12 minutes per orbit. Each operation sequence must be longer than 1 minute and no more than 4 operation sequences are possible per orbit.

The AMI wind mode and wave mode can be operated separately.

Simultaneous operation of wind and wave mode is provided in the interleaved wind/wave mode. All performances and programming capabilities provided for the sequence is interrupted every 30 seconds for a duration of two FMA sequences to permit wave operation.

The only constraint on realising the maximum duration of operation in wind, wave or interleaved modes is the on-board energy resource limitation.

Both wind and wave mode data are recorded on-board.

The Wind Scatterometer

Functional Blockdiagram

The AMI functional blockdiagram for wind mode is shown in Fig. 4.

Transmitter

A detailed block diagram of the transmitter is shown in Fig. 5. The lower and the central parts are used for Imaging and Wave modes whereas the upper and the central parts are used for Wind mode.

When operated in Wind mode, the Active Microwave Instrument (AMI) uses the same Centre frequency (5.3 GHz) and the same peak power (~ 5 kW) than in SAR imaging mode, but the type of modulation is different.

The transmit signal is a pulsed RF carrier with constant frequency (Rectangular Pulses as shown on Fig. 6) switched sequentially between the three scatterometer antennae (fore, mid and aft).

To take into account the different geometry for the side antennae (fore and aft) and for the mid antenna as

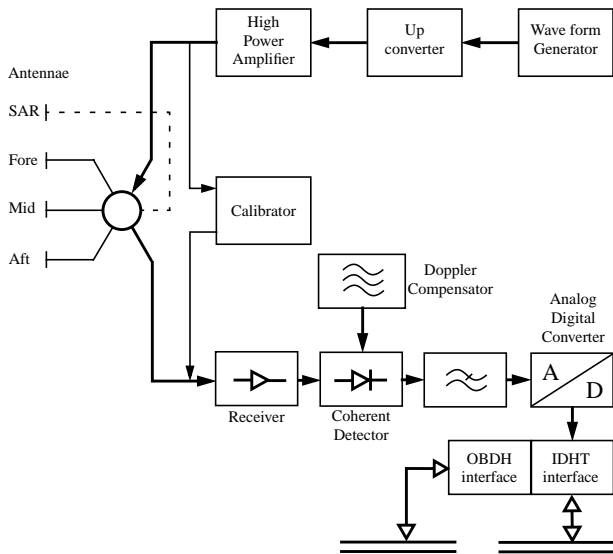


Figure 4: Scatterometer functional block diagram

shown on Fig. 1, the pulse length and pulse repetition frequency are the same for the side antennae but are different for the mid antenna.

A rectangular pulse of 130 s for the Side Antennae and 70 s for the mid antenna is generated at an IF of 123.2 MHz. with a respective pulse repetition interval of 10.21

20 dB / div (within pulse)

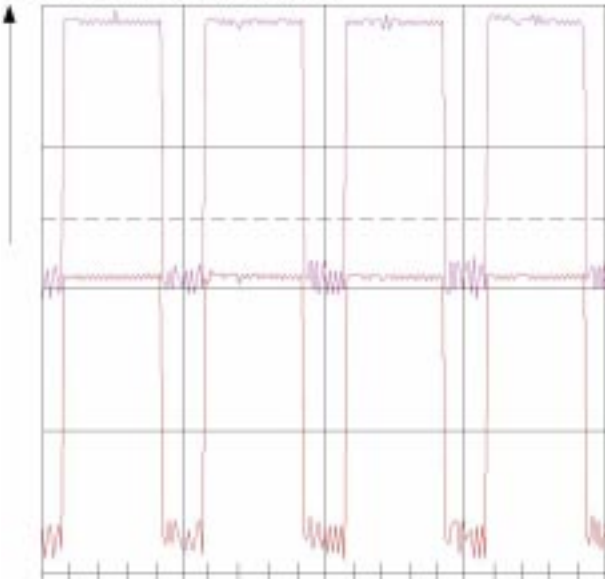


Figure 6: Example of scatterometer pulses as measured on ground during instrument testing

ms and 8.7 ms. The upconverter shifts this signal in frequency up to 5300 MHz. The required high RF output power is produced by the HPA (High Power Amplifier) which contains a TWT (travelling Wave Tube) as the

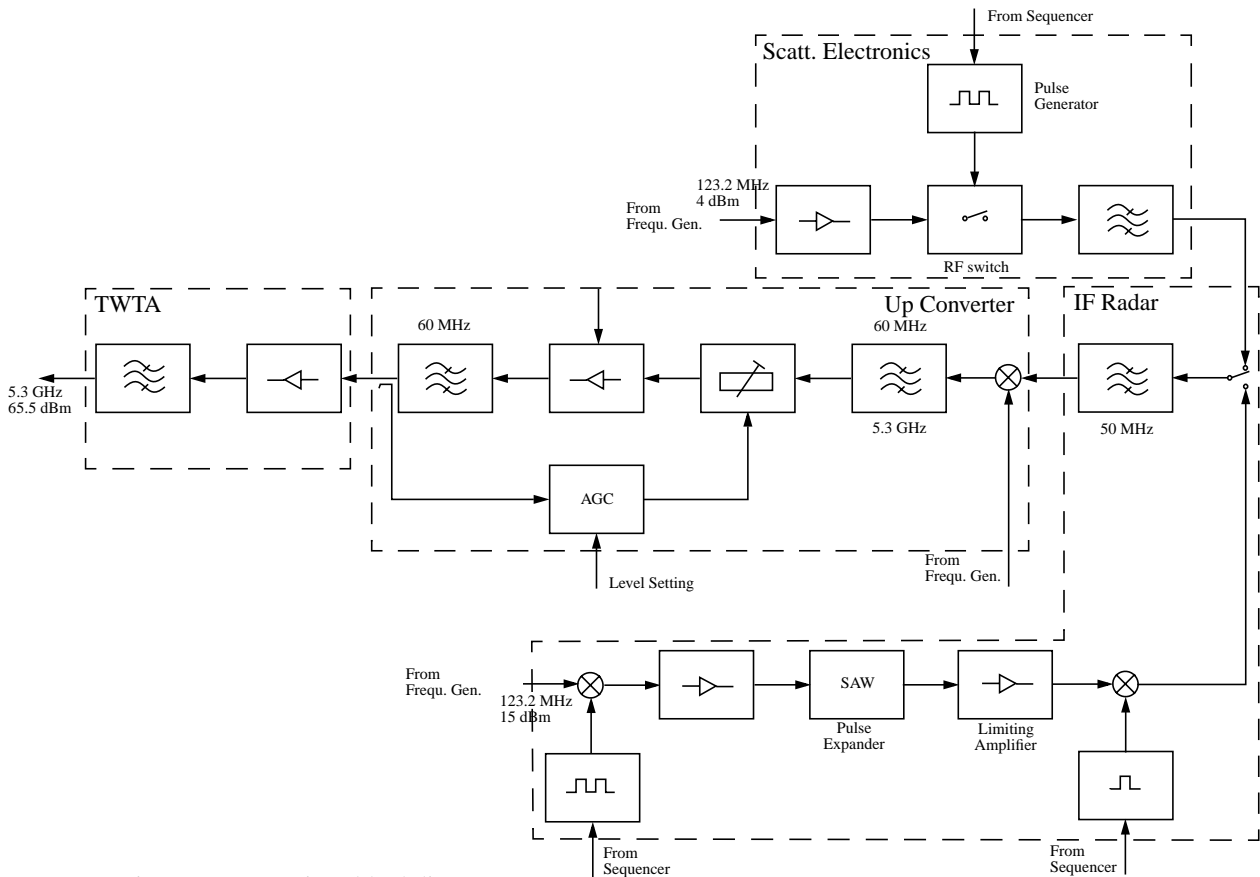


Figure 5: Transmitter blockdiagram

amplifying device. An automatic level control loop within the upconverter maintains the TWTA input power at a constant level adjusted to drive the TWTA just well into saturation. The mean RF output power within pulse measured at the HPA Waveguide flange is at least 65.5 dBm.

Scatterometer Antennae

The scatterometer antennae are planar waveguide arrays connected to the transmitter and the receiver via the circulator assembly (switch matrix). The measured antennae boresight gains (for ERS-2) are 30.6 dB, 28.0 dB and 30.9 dB respectively for the Fore, Mid and Aft antennae. The cross polarisation is more than 40 dB below the maximum co-polarisation for each antenna. The fore and aft antennae are identical in shape but have a different pointing, respectively 45 ° and 135 ° with respect to the flight direction.

Calibrator Sub-System

The calibrator is aimed at deriving highly stable, delayed and amplitude scaled samples of the transmitted pulses. The analysis of these calibration pulses at the receiver output permits the monitoring of the product of the transmitted power and the receiver gain, and to compensate for it (see Fig. 7) [3].

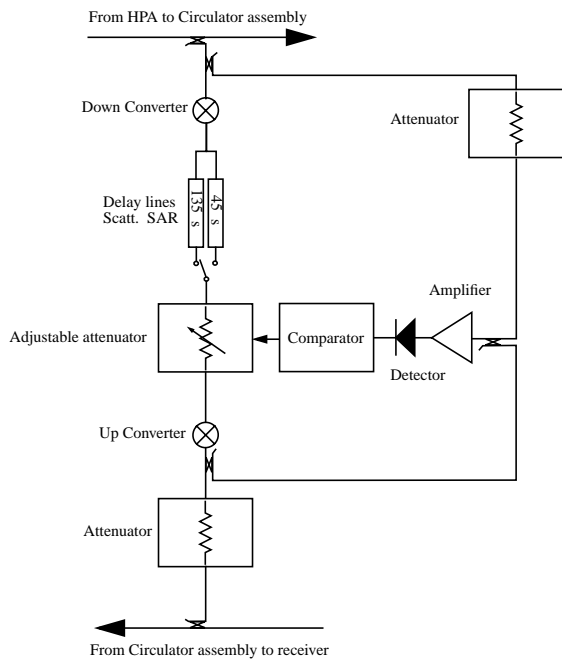


Figure 7: Basic elements of the AMI Calibration S/S

Scatterometer Measurements

After reception of the return echoes, the signal is filtered and a non-coherent detection is performed on-board still in the form of I and Q components and for each antennae separately. The doppler compensators remove the frequency shift placed upon the receive sig-

nal due to the motion of the spacecraft and the beam look direction (mainly for the fore and aft antennae). The I and Q components are converted into digital codes and telemetered to ground via the IDHT (Instrument for Data Handling and Transmission) interface. Due to the higher dynamic range requirements in Wind mode the A/D converter has a finer resolution in Wind mode (8 bits) than in Imaging mode (only 5 bits). For radiometric stability and accuracy purposes more gain drift calibration pulse and noise measurements are performed in Wind mode than in the other modes.

Timelining

The three scatterometer antennae, fore (F), mid (M) and Aft (A), are operated in sequences of 32 Radio Frequency pulses each, starting with the fore antenna as shown in Fig. 1. The Pulse Repetition Interval (PRI)

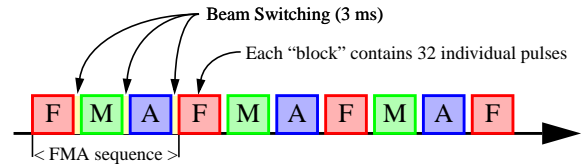


Figure 8: Scatterometer Beam Switching sequence

being of 10.21 ms for the side antennae and of 8.7 ms for the mid antenna, the total length of a repeat cycle called a FMA sequence is 940.84 ms as summarised in Table 3.

Table 3: Timelining Diagram for Wind mode

Fore Antenna	32 x 10.21 ms	326.72 ms
Switching		3.00 ms
Mid Antenna	32 x 8.70 ms	278.40 ms
Switching		3.00 ms
Aft Antenna	32 x 10.21 ms	326.72 ms
Switching		3.00 ms
Total of one FMA sequence		940.84 ms

Four FMA sequences last 3.763 seconds and correspond to 25 km along the sub-satellite track when the satellite is at an altitude of 785 km and is continuously repeated in the Wind with any gaps.

The fixed duration of this sequence means that it does not always correspond exactly to 25 km along the sub-satellite track as the satellite altitude varies over the total ERS orbit from 769 km to 825 km, and with the altitude, the relative velocity of the spacecraft to the ground.

Gain drift calibration pulse measurements or noise measurements are taken after each transmit pulse before the echo signal returns. During each beam sequence of 32 pulses, 4 gain drift calibration pulses and 28 noise signals are measured (see Fig. 1). In the calibration unit, the gain drift calibration pulse is delayed by 135 srela-

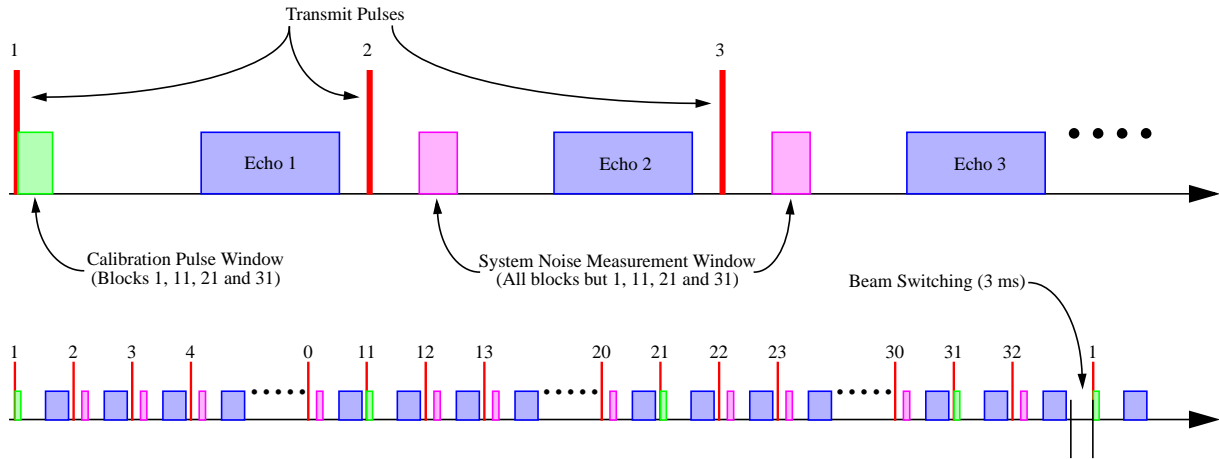


Figure 9: Sequence of 32 Scatterometer transmissions

tive to the transmit pulse in order to fall in the Calibration window.

Table 4 summarise all the pulse and sampling characteristics.

Table 4: Pulse and sampling windows characteristics in Wind mode

Parameter	Fore and Aft beams	Mid Beam
Pulse Shape	Rectangular	Rectangular
Pulse width	130 μ s	70 μ s
Pulse Repetition Interval	10.210 ms	8.700 ms
Sampling rate	30 kHz	30 kHz
Number of bits for I & Q	8 bits	8 bits
Number of samples	Echo Signal	118
	Cal. Pulse	30
	Noise	32
Calibration Window start	100 μ s	100 μ s
Calibration Pulse Delay	135 μ s	135 μ s
Length of Cal. Window	1.000 ms	1.000 ms
Noise Window start	1.500 ms	1.500 ms
Length of Noise Window	1.030 ms	1.030 ms
Echo Window start	5.400 ms	5.200 ms
Length of Echo Window	3.910 ms	2.440 ms

Doppler Compensation

The radar echo from a target on the earth's surface doesn't always have the same frequency as the transmitted signal because of doppler shifts, due to the relative motion between the satellite and the target. This motion depends on satellite velocity, antenna look angle and earth rotation.

The range of the doppler shift is 50 - 150 kHz for the side antennae and 0 - 10 kHz for the Mid antenna. By yaw - steering the satellite, the doppler shifts in the mid - antenna are minimised but not entirely eliminated. It follows from the above that continuous frequency tuning of the scatterometer receiver is required to keep the echo signals within the 25 kHz on-board bandwidth.

The frequency deviation is not only function of the echo time delay, but varies also over the orbit due to geometrical effects and earth rotation.

Nominally, every 15 s the on-board doppler correction is updated, but provision are made that no update takes place during a 32 pulses sequence of a single beam.

The required tuning signal is synthesised on-board by the scatterometer electronic module, using a time dependent algorithm with coefficient provided to the instrument by macrocommand.

The accuracy with which the received signals are actually centered within the receiver band depends on the pointing errors, the receiver hardware errors, the computational and curve-fitting errors (for the on-board compensation)+, as well as the uncertainties introduced by the geometry such as earth and orbit modelling.

These errors have an effect on instrument radiometric stability. The on-board errors are partly compensated by the on-ground filter and fine tuning algorithms of the Wind mode processor. The actual receiver tuning errors are limited to a small fraction of the 25 kHz receiver bandwidth.

The blockdiagram of the scatterometer detector and doppler compensator is shown in Fig. 10.

Receiver gain Setting

The receiver Gain is set differently for the Side and the Mid antenna in order to take into account the different bandwidth of the signal due to the geometry of the system.

The nominal receiver gain, both for ERS-1 and ERS-2 is -111.7 dBW for the Side beams and -106.6 dBW for the Mid beam. Because of the reduce transmitted power required for ERS-2 the Receiver gain was respectively set to -112.6 for the Side antennae and -107.91 for the Mid antenna.

Sampling

The echo, as well as the calibration pulses and the noise, are sampled at 30 kHz. The Analogical to Digital

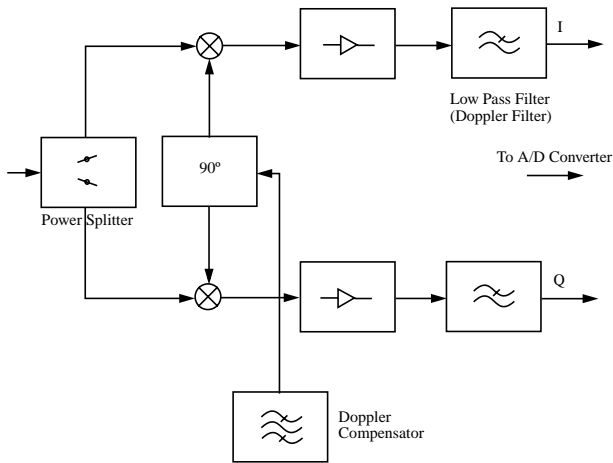


Figure 10: Scatterometer Detector / Doppler

converter is making instantaneous measurement of the input signal. This sampling rate corresponds to roughly 5.2 km at 18° incidence angle (Mid beam, inside the swath) and 13.3 km at 68° incidence angle (side antennae, far swath).

Interface to the Instrument for Data Handling and Transmission

All echo and calibration data are directly transferred to the IDHT without any on-board processing, whereas the noise data are pre-processed on-board by software. In fact all noise samples are averaged over each 32 shot sequence. This means that the 32 noise samples per sampling window multiplied by the 28 noise sample windows, which results in 896 noise samples are averaged on-board. the averaging is made separately for the I and the Q channel. the averaged noise data is then included as a 16 bit word for I^2 and for Q^2 as part of the auxiliary data stream.

The data are transferred to the IDHT in form of source packets. Each source packet includes the data collected during 32 shot beam sequence. The generation time for a source packet is therefore 326.72 ms for the side antennae and 278.40 ms for the mid antenna. The IDHT will read out at a mean data rate of 1.09 Mbit/s one source packet in a time not greater than 280 ms. The IDHT stores and transmits the measurement data in the same sequence in which it was sampled.

It is important to note that the Mid antenna source packet differs from those of the Fore and Aft antennae by the fact that less echo data are present (74 instead of 118). To obtain three source packets of the same size, 7860 bytes, dummy data are inserted at the end of the Mid packet.

Source Packet Description

Each source packet is composed of three parts, the primary and secondary headers and the measurement data field.

The primary header contains three fields:

- the Packet Identifier containing in particular the antenna id and the operation mode (Wind, Wind/Wave or calibration mode).
- the Packet Sequence Control coded over two bytes. This parameter is restarted after each switch-on in that mode and labels each individual FMA sequence. Then after switch-on the Source packets will be labelled 0, 0, 0, 1, 1, 1, 2, 2, 2, ...etc...
- The source packet length fixed to 1EAD (HEX) which correspond to 7854 bytes (from 0 to 7853) and doesn't include the 6 bytes of the primary header.

The secondary header contains the time code given by the ICU (Instrument Control Unit) and the auxiliary data.

The time data included in a source packet shall have a known relationship to the actual time at which the data contained in that packet is sampled with an accuracy of 1 s. The time data is sampled 10.210 ms (-1, + 250 s) for the side antennae and 8.700 ms (-1, + 250 s) for the Mid antenna after the last RF transmit pulse leading edge (Fig. 1).

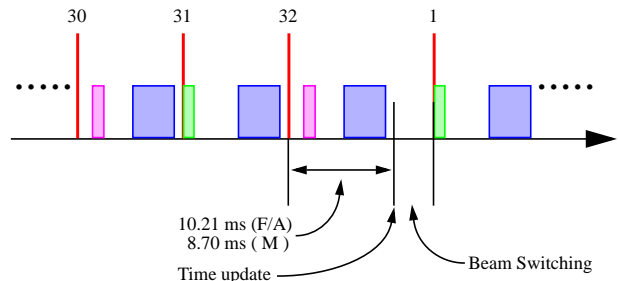


Figure 11: Sampling of the time code

The auxiliary data supply the additional information needed for the interpretation and the processing of the measurement data. In particular the following information is included:

- Scatterometer time from the ascending node (the resolution is $1/256 = 3.90625$ s). Reset to zero at each ascending node.
- Scatterometer Calculation time used for the on-board doppler compensation. Updated every 15 s.
- The orbit period used to reset the scatterometer and the scatterometer calculation times.
- All the instrument setting (gains, modes Attenuations, doppler coefficients).
- The noise measurements for I^2 and Q^2 coded over 16 bits.

The measurements data simply all the I and Q samples coded over 1 byte for the following measurements:

- 1st Calibration Pulse
- 1st to 10th Echoes
- 2nd Calibration Pulse
- 11th to 20th Echoes
- 3rd Calibration Pulse
- 21st to 30th Echoes
- 4th Calibration Pulse
- 31st to 32nd Echoes

Which corresponds to 7792 bytes for the Fore and Aft antennae and 4976 bytes for the Mid antenna.

2816 bytes of dummy data are added to the Mid antenna source packet in order to have a total of 7796 for the measurement data field.

Scatterometer Data Characteristics

It is interesting to have a description of the three major parameters included in the source packets, namely the noise measurement, the calibration pulse and of course the echoes. These measurements are given in ADC units which correspond to one step of the Analog to Digital Converter.

The noise measurements

Each source packet contains one average of the I^2 and Q^2 noises estimated from the $32 \times 28 = 896$ I and Q noise samples retrieved during one measurement block. Typically this value is 1 ADC step for the Fore and Aft antennae and 0 for the Mid Antenna as it is shown on Fig. 1. The averaged values since ERS-2 scatterometer started operation are stable as summarised in Table 5.

Table 5: ERS-2 Scatterometer I and Q noise value

Fore Antenna		Mid Antenna		Aft Antenna	
I	Q	I	Q	I	Q
0.97403	0.88831	0.00000	0.00000	0.92508	0.81170

The instrument noise is so low that it never exceed one quantisation step for the side antennae and is always set to 0 for the Mid beam. This fact is confirmed on Fig. 1 which shows the evolution of the noise levels during the overall ERS-2 scatterometer operation (23 November 1995 - 17 August 1998).

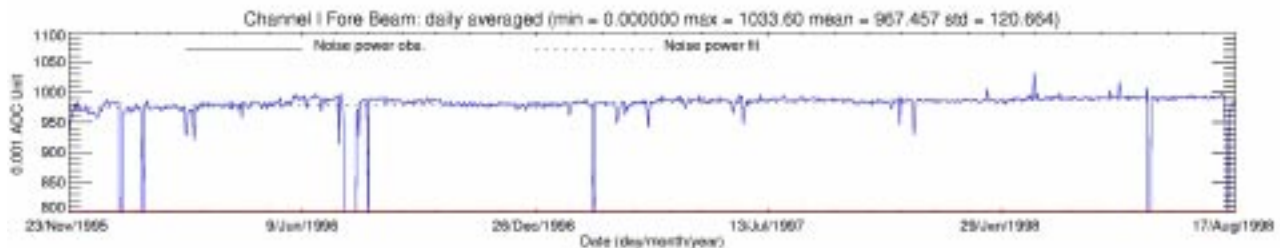


Figure 13: ERS-2 scatterometer noise level evolution since the beginning of the mission (23 Nov. 1995 - 17 Aug. 1998)

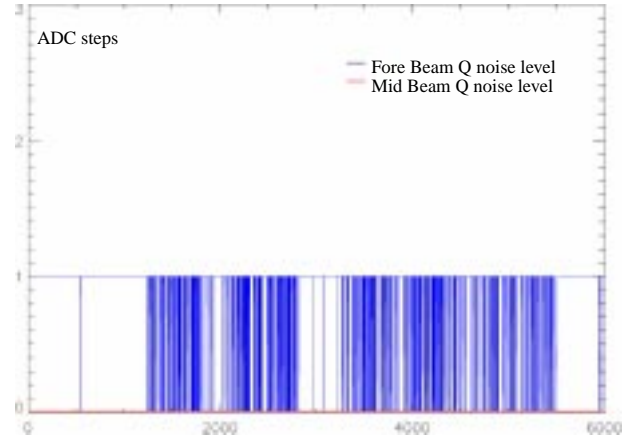


Figure 12: Typical Fore and Mid noise measurements for a complete orbit every FMA sequence (every 904.8 ms).

When this level of noise is compared to the level of the echoes (Fig. 14 and Fig. 14), the reason why no negative values of the σ^0 are never extracted from the ground processor, especially after the spatial filtering (see the related paragraph hereafter), becomes very clear.

An other discussion on the overall system noise can be found annexed to this report (not yet included).

The calibration pulses

The calibration pulse is an image of pulse sent toward the ground. It is an important element of the data for two reasons. First, it used to normalise the returned echo in order to correct for any short term or long term evolution of the High Power Amplifier. Second, it is permanently and very closely monitored in order to anticipate instrument ageing and to detect anomalies.

Table 4 gives the main characteristics of the calibration pulse (130 and 70 respectively for the Side and Mid antennae, delayed by 135 s) and of the Calibration window (it starts 100 s after the pulse and it is sampled at 30 kHz). A schematic of the pulses (Side and Mid antennae) at the output of the HPA, of the calibration pulses delayed in the calibration sub-system and low pass filtered and of what would be the sampling of this later pulses is given in Fig. 14 and Fig. 14. The comparison with typical pulses actually measured are shown on Fig. 14.

If the sampling of the calibration pulses doesn't allow for a detailed analysis of the pulse shape or of the low

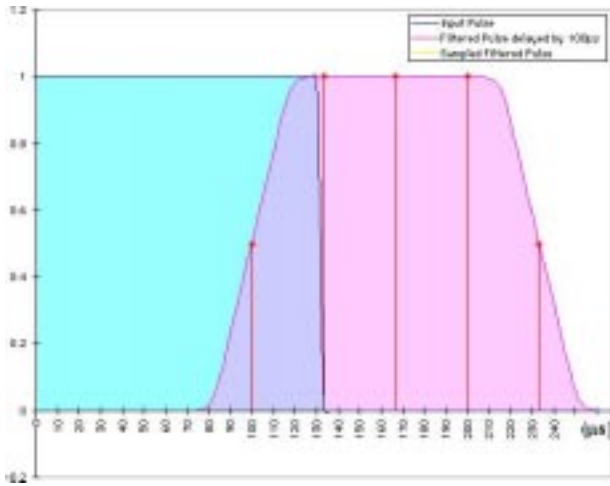


Figure 14: Fore Calibration Pulse Timing and sampling

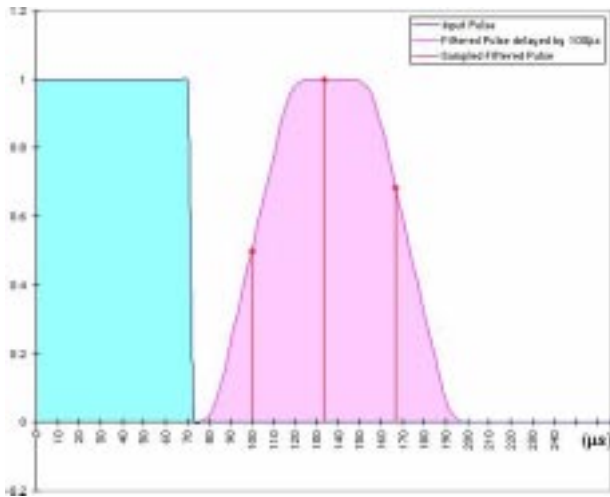


Figure 15: Mid Calibration Pulse Timing and sampling

pass filter, it certainly allows to monitor the HPA power and the instrument timing.

It is important to remember that, due to the reduction of power required to operate the ERS-2 AMI, the TWTA

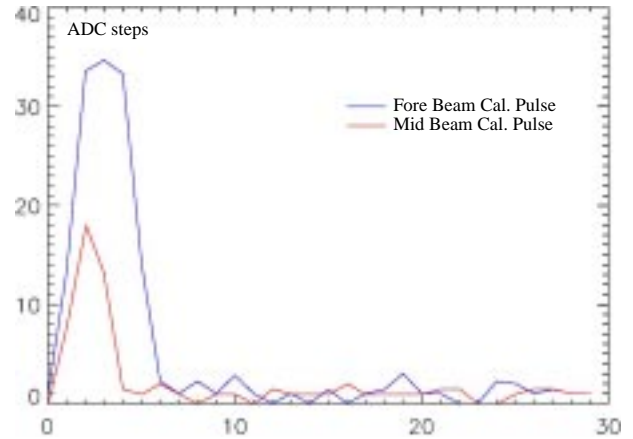


Figure 16: Typical Fore and Mid Beam Calibration Pulse

is not working in saturation. Therefore, any variation of the pulse's power (due to pulse generator for example) will be seen in the transmitted pulse and in the echo.

In this context it becomes very important to monitor very closely the ERS-2 Calibration pulse power in order to assess evolution of the transmission part of the instrument. The same monitoring for ERS-1 never showed any evolution of this part of the instrument.

Fig. 17 shows the evolution of the Calibration Pulse power evolution since the beginning of the ERS-2 AMI mission (23 November 1995 - 17 August 1998). It is clear that the power is decreasing by roughly 0.14 dB per cycle since the Calibration Sub-System B is operational used (August 1996). It seems that the slope was slightly smaller when the sub-system A was in used. This power decrease is automatically corrected for during the on-ground processing.

The echoes

The returned echoes are sampled at a rate of 30 kHz which correspond to roughly 10 km on ground (see Sampling), after the doppler compensation and the low pass filter.

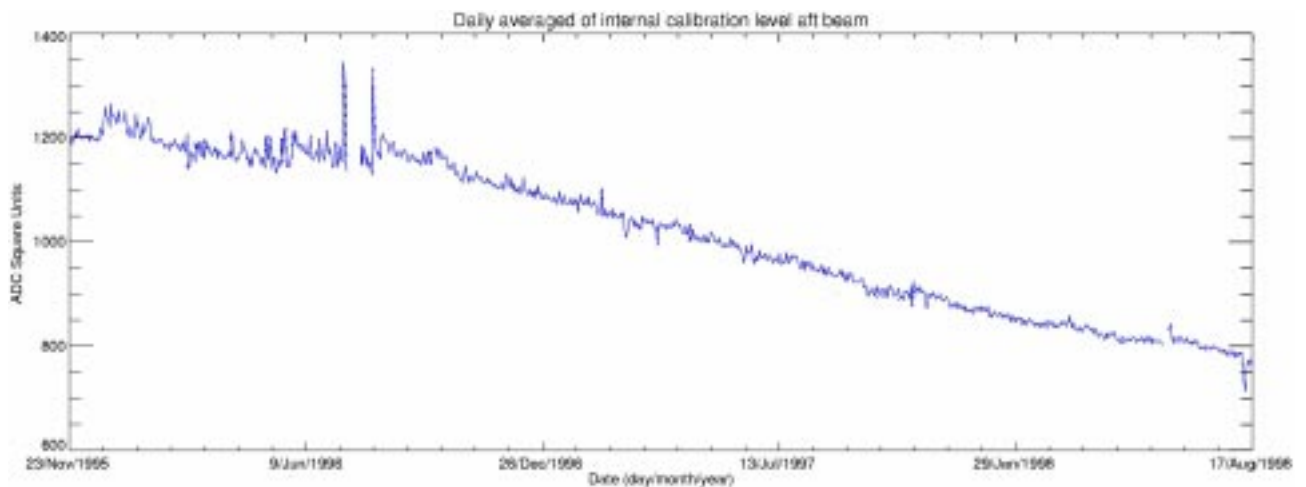


Figure 17: ERS-2 scatterometer calibration pulse power evolution since the beginning of the mission

Fig. 14 and Fig. 14 are respectively showing Fore and Mid antenna echoes over ocean (East Tropical Pacific) before any processing on ground and for comparison, Fig. 14 and Fig. 14 are showing a Fore and mid antenna echo over ice (North of Alaska during the winter 97-98).

Because of the different gains used for the Side and Mid antennae, the power level of the Mid beam is half than of the Side beams.

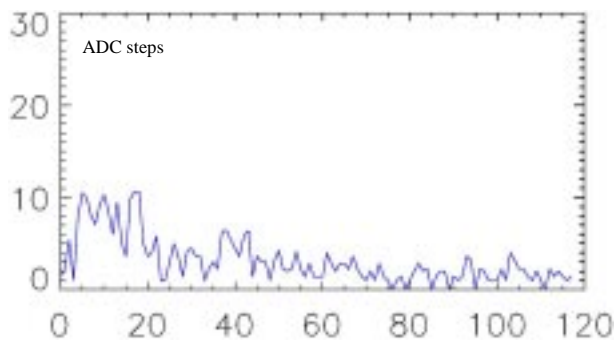


Figure 18: Typical Fore Beam echo over ocean

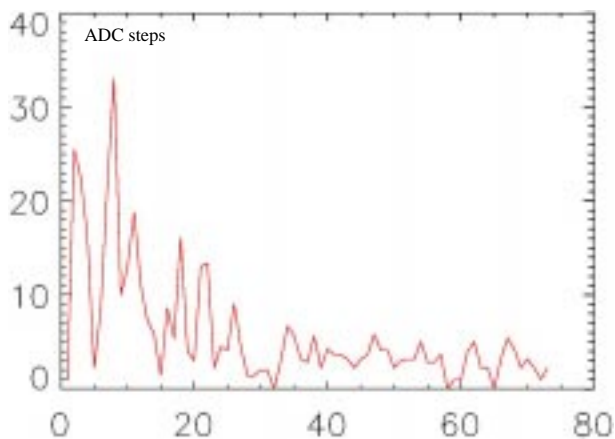


Figure 19: Typical Mid Beam echo over ocean

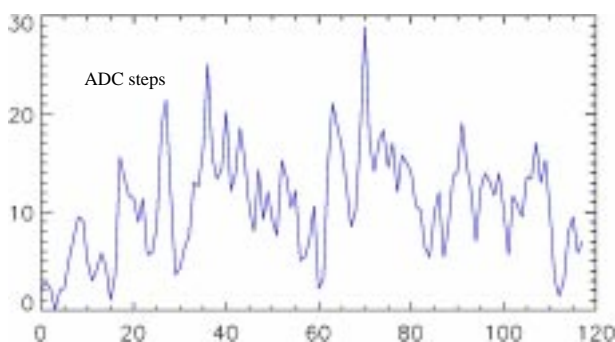


Figure 20: Typical Fore Beam echo over ice

Scatterometer Processing to σ°

Performances

The performance of the scatterometer is defined in terms of:

- swath coverage
- localisation
- σ° measurement range and stability
- output signal response to a fictive point target (both in time and frequency domain)

In order to achieve the required overall performances, the measurement data delivered by the instrument have to be processed on-ground using externally supplied data (orbit and attitude information) and the characteristics of the instrument (instrument characterisation data).

Input Data

The input to the processing are of three major types. The instrument delivered data (target data, noise, internal calibration and time information), data delivered by the orbit propagator and the external data containing the relevant information on the instrument characteristics, the system geometry and the ground processing.

The instrument data have been described in the previous chapter. The orbit propagator is included in the processor and is used to relate acquisition times and satellite and targets localisation around the earth using the Goddard Earth Model (GEM6) for earth surface modelling.

Generally, other external data not computed with the orbit propagator are provided as Look-Up-Tables as either a scalar or an array and can be updated, if the need arise, in particular when new calibration coefficient, antennae pattern or orbit characteristics. These tables may depend on the beam activated and may be indexed by the orbit time and the pulse time.

All these tables are provided by using the Scatterometer Simulator System (SSS). An important part of the scatterometer data processing is done before hand in the SSS and is passed to the real-time processor via these Look-Up-Tables. This includes mainly the Doppler compensation phases, the normalisation factors used to convert the powers into σ° (both for the echo and for the noise) which are computed using the antenna patterns, the incidence and look angles.

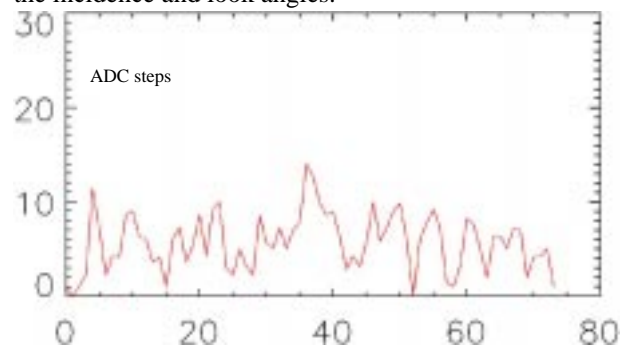


Figure 21: Typical Mid Beam echo over ice

Output Data

The output data includes:

- the node characterisation data
- the σ^o values
- the k_p values (standard deviation of each σ^o estimate)
- the product confidence data (monitoring parameters and processing flags)

The node characterisation data comprises the node position in latitude and longitude which is directly computed using the orbit propagator and the node incidence and look angles which are derived from the Look-Up-Tables.

The σ^o are the primary output from the scatterometer ground processing. They are the main input to the σ^o to wind conversion, but are also used to directly for land and ice applications.

The standard deviation k_p of each σ^o estimate computation is based on the following two assumptions. This parameter is dominated by the instrument noise and not by the speckle, an approximation to within 20% is adequate.

The product confidence data are used to monitor the system behaviour (power spectrum monitoring, I/Q imbalance monitoring, internal calibration level monitoring) as well as processing flags (valid/invalid, arcing, ...etc...).

Main processing steps

A functional block diagram of the scatterometer Ground Processing is shown on Fig. 1.

The main processing steps to be performed are listed in sequence below:

- Resampling and filtering of the measurement data delivered by the instrument to avoid aliasing during later processing steps and to compensate for the on-board filtering,
- Doppler compensation to shift the spectrum of the received signal into the low pass filter passband,
- Low pass filtering to improve the signal to noise ratio,
- Envelope detection to get a measure for the signal power,
- Block averaging to reduce both the data throughput for the following steps and the variance of the signal power samples,
- ADC-non linearity correction
- Noise correction to increase the measurement accuracy,
- Internal calibration correction to compensate for the transmitter and the receiver fluctuations,
- Power to σ^o (radar Backscattering coefficients per unit area) conversion to relate the measured signal power to the wanted quality σ^o ,
- Spatial integration both to increase the measurement accuracy (radiometric resolution) and to give the desired point target response,

- Output signal characterisation (including the estimation of the k_p) to allow the determination of wind characteristics from the ground processing output data,
- Product confidence check to monitor the accuracy of the on-board and the on-ground doppler compensation process, the I/Q channels imbalance and the internal calibration time delay.

Description of the main processing steps

Resampling and Refiltering

The target data entering the ground processing in form of I and Q components, are sample values of a continuous time function. In order to avoid aliasing (Nyquist's criterion), the sampling frequency is chosen higher than twice the highest component contained in the spectrum of the input function.

The next step in the processing is the doppler compensation which consists in a multiplication in the time domain. Depending on the Doppler compensator frequency, this multiplication can cause a slight frequency spread. In order to avoid aliasing in case the sampling frequency is just adequate for sampling the input function, the signal should be resampled at an increased rate before the doppler compensation function is called.

It was chosen to perform the resampling in the frequency domain with the help of two Fourier transforms. The correction for the on-board filter ripples, the resampling step is combined with a refiltering, which is performed by multiplying the signal spectrum with the appropriate filter transfer function.

The spectral shift which could occur during the extension of the complex spectrum and the refiltering is avoided by using two real-to-complex and real-to-complex FFT's instead of single complex-to-complex FFT's.

Doppler Compensation

The Doppler compensation aims at compensate for the Doppler shift introduced on the received signal due to the motion of the spacecraft and to the earth rotation. Most of the original doppler shift of the echo signal is compensated on-board, in a dedicated mixer stage within the instrument, by the application of a suitable time dependant local oscillator signal. The Doppler compensation itself is simply a multiplication in the time domain. The difficulty associated with Doppler compensation is the complicated law governing the Doppler frequency versus echo time behaviour and its change over the orbit due to:

- non-circular orbit,
- rotating oblate earth,
- spacecraft attitude steering,
- on-board compensation Doppler law.

The Doppler compensation information is contained in an externally supplied 2-dimensional Look-Up-Table. In order to reduce the computational load on the ground

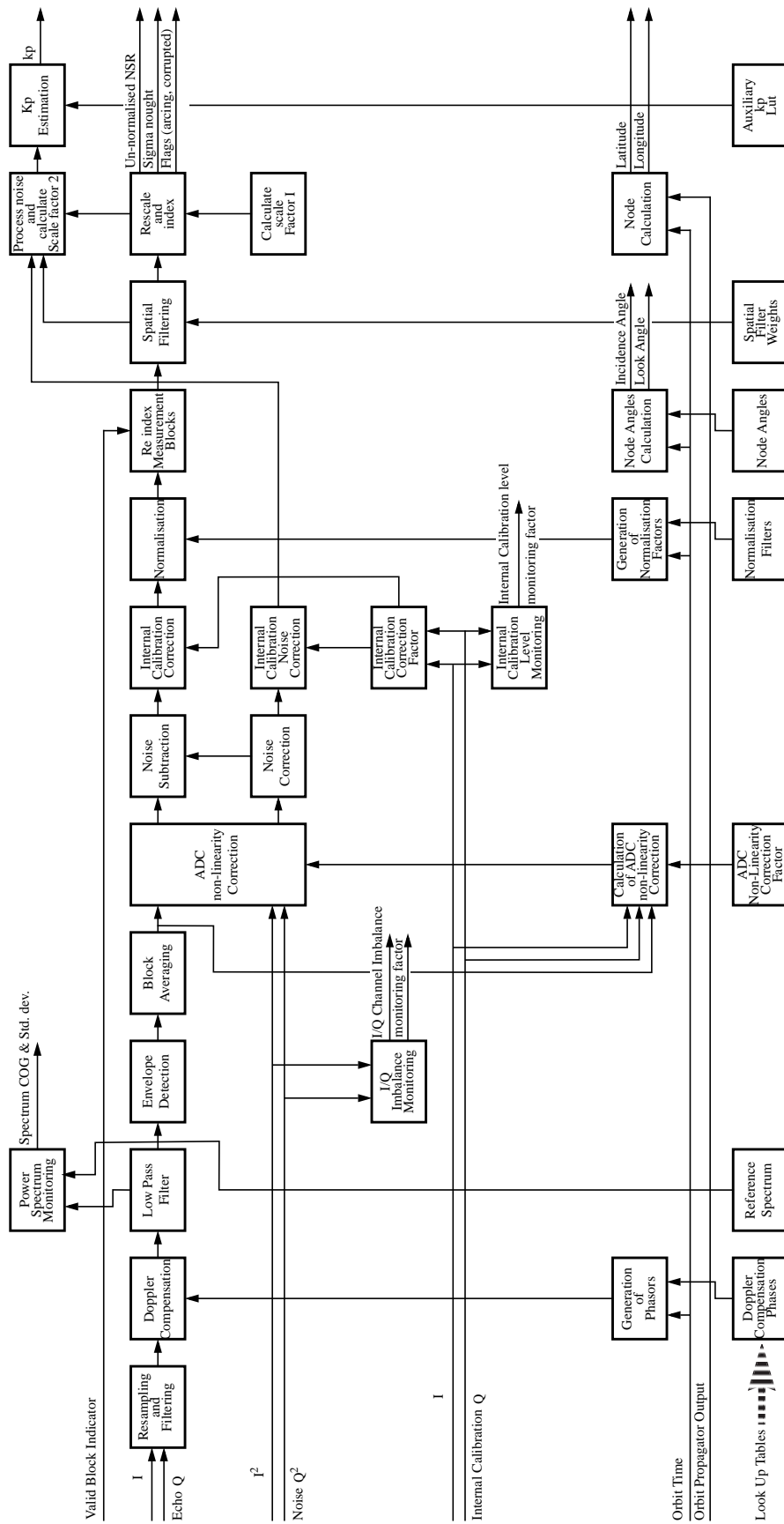


Figure 22: ERS-2 scatterometer Ground processing Functional Block Diagram

processing, this Look-Up-Table contains the phase rotation to be applied to the signal samples rather than the residual Doppler frequency shifts.

Low Pass Filtering

The aim of the low pass filter after the Doppler compensation, is to match the overall system bandwidth of the received signal in order to optimise the signal to noise ratio. The signal bandwidth is changing with the time along the echo (see Sampling above) and the position along the orbit, but the effect is relatively small and therefore the filter function is defined time-independent. The filter function is defined in the frequency domain and here to the most effective way is to perform the low pass filtering is by using FFT's and multiplication in the frequency domain. During this operation, it was taken care of avoiding any aliasing in the time domain due to insufficient sampling in the frequency domain and to the extension of the signal in time caused by the low pass filtering.

Envelope detection

Up to the output of the low pass filter, the signal is represented as I and Q (in phase and in quadrature) signals. The instantaneous power is calculated by summing the square of each I and Q samples.

Block Averaging

The duration of a measurement block is roughly 300 ms (see Table 3), and the corresponding distance measured on the sub-satellite track is roughly 2 km. This distance is small compared to the diameter of the spatial integration area (in the order of 100 km) and therefore corresponding target samples (those with identical echo time) can be averaged over the 32 echoes before further processing in order to reduce the data throughput.

The time instant appointed to the block signal is the average of the time instants for the 1st and the 32nd pulses of the block which is averaged. It has to be noted that these times are not directly provided in the raw data, but are derived by using the information illustrated on Fig. 1.

ADC Non-linearity Correction

In theory, the signal power (both echo and noise) at the ADC can be such that a significant proportion of samples exceeds the ADC maximum level, or is below the least significant bit level, a significant sampling error occurs. This is not reduced by sample averaging and there is a resultant power transfer non linearity. These value of non linearity are comparable with the required radiometric stability, so will have to be corrected for during the ground processing. Since this is a statistical correction to the power, it should be applied after the power detection and the block summation.

In practice, the echo is fairly low in the ADC (less than 40 ADC steps) and the noise is always 0 or 1 ADC

step (see Chapter on Scatterometer Data Characteristics).

This ADC non-linearity correction is performed for both the block averaged target echo and the noise averages.

The Analogical to Digital Converter non-linearity is characterised on-ground and provided to the ground processing via a Look-Up-Table, which for a given ADC output power gives a correction factor to be applied in order to retrieve the expected input power.

For ideal correction, the output power used to determine this correction factor should be obtained immediately after the ADC. In order to reduce the stochastic variance of individual power samples a running average over the corresponding echo power samples of the last 8 measurement blocks of the same beam is performed.

A more precise value of the correction factor is derived by linear interpolation between two successive readings of the LUT.

The correction factor for the noise power correction is based on the actual averaged noise power only.

Noise correction and subtraction

The target signal is masked by the receiver noise, or more precisely, the signal power which is measured is the signal power plus the receiver noise power. To improve the instrument accuracy, the receiver noise power is measured separately and then subtracted from the sum of both. The processing required for noise subtraction is partly performed on-board (see The noise processing above). The I and Q channel averages (I^2 and Q^2 averages) are added on-ground to derive a single noise power estimate. This noise sample is used to correct each individual target sample of the corresponding measurement block by simple subtraction. Just before the subtraction, the noise is multiply by a constant which takes into account the different ways of noise processing in the target measurement chain and the noise chain. This constant depends on

- the receiver pre-doppler compensation transfer function,
- the frequency offset applied by the on-board Doppler compensation for the noise alone measurement,
- the on-board low pass filter,
- the on-ground detection filter.

This constant is supplied externally.

Internal Calibration Correction and HPA monitoring

During internal calibration, a small fraction of the transmit signal is directly routed into the receiver low noise amplifier via a calibrator. The main function of the calibrator when the AMI is in scatterometer mode is to delay the transmit signal a little bit more than the transmit pulse length to allow sampling of the delayed signal at the output of the receiver. During each measurement block, four calibration measurements take place after transmit pulses 1, 11, 21 and 31. Within the receiver, the

samples taken during the calibration window are handled in the same way as the target samples. They are transferred to the ground as I and Q components. After proper processing on-ground, they are used to correct for gain variations and to monitor power level variations of the instrument.

No on-ground Doppler compensation and no low pass filtering is required for the internal calibration signal. After forming the envelope squared of the signal ($I^2 + Q^2$), gain information is extracted. In order to reduce quantisation noise, the result is low pass filtered by an exponential filter.

As the envelope squared of the signal is rather sensitive to deviations of the characteristics of the I and Q channels from the ideal case, a possibility to correct the calibration signal samples for these I/Q imperfections, based on an externally provided characterisation, is foreseen.

The gain correction information is derived as a multiplicative correction factor which is applied to the noise corrected signal samples. This factor is the ratio of the actual low pass filtered internal calibration signal energy and a reference energy valid for that system configuration which was used to derive the normalisation factors.

Noise correction is not required for the calibration signal due to the high signal to noise ratio.

The averaged energy of the four calibration pulses of each measurement block is used to detect missing transmit pulses due to the arcing of the High Power Amplifier (HPA). If HPA arcing occurs the HPA is switched down and automatically restarted after a few seconds, unless the number of arcing exceeds a certain threshold, which leads to an error condition of the AMI. During HPA switch down, no transmit pulses and hence no internal calibration pulses are generated and therefore only noise is recorded during the internal calibration and echo sampling windows. The σ^0 derived from these echo samples are invalid and have to be flagged accordingly. As the noise energy is much below the internal calibration pulse energy, HPA switch down can be detected by comparing the averaged energy of the samples of the calibration pulses of a measurement block with a threshold value and raising a flag for those measurement blocks, for which the averaged energy is below the threshold. These flags are used during the spatial filtering to determine the nodes affected.

Power to σ^0 Conversion - Normalisation

The target signal at the output of the envelope detection is proportional to the instantaneous power. The quantity to be measured is the backscattering coefficient σ^0 . In order to perform the desired spatial integration of the σ^0 values around the node, the measured power needs to be converted into σ^0 .

The normalisation factor is defined as the instantaneous power at the input of the normalisation block for a uniform reference backscatter coefficient equal to 1 on

the earth surface everywhere in the swath. Due to the changing geometry with the time of the echo (beam range) and along the orbit, this normalisation factor for a given antenna, is a function of both variables.

Initially, provision was made to correct for the variation of the scatterometer antennae temperature around the orbit, which would have caused a mechanical distortion of the antenna and a modification of the antenna pattern. Practically this capability was never used and a unique set of normalisation factors were used (for a given orbit characteristic and antenna pattern).

The ERS scatterometer system is far from being simple from the point of view of the geometry as well as from the point of view of the instrument.

These normalisation factors are supplied externally as Look-Up-Tables indexed by the orbit time and the echo time. The values not contained in the LUT's are calculated by bi-linear interpolation.

Spatial Filtering

The spatial filtering process consists of two different steps:

- Calculation of the node positions on the earth's surface in an adequate coordinate system,
- weighted integration of samples belonging to an area around these nodes (integration area).

The weighting function used and the size of the integration area are mainly determined by the scatterometer system requirements in terms of the instrument response to a point target on ground, specified both in the time domain (impulse response) and in the frequency domain (modulation transfer function). The integration process acts like a two-dimensional filter, hence the name "Spatial Filtering".

The calculation of the node position is based on the Mid antenna measurement blocks.

The position of the central node of the swath (node 10) is at the intersection of the Mid antenna line of sight with the earth (defined by GEM6) (see Fig. 23). The other nodes are localised along the intersection of the plane defined by the centre of the earth, the satellite and the Mid antennae line of sight every 25 km in both directions. A total of 19 nodes are localised like that for a given Mid antenna measurement block. This is repeated every four measurement blocks (equivalent to four FMA sequences), which corresponds to 3,763.36 ms or roughly 25 km on ground. It has to be noted that because of the oblateness of the earth, these successive line of nodes are not exactly parallel.

The results of this process is shown on Fig. 24. Samples taken by the three antennae within a certain area around each node are averaged. The averaging process gives a high weight to the samples near the node and a low weight to those far from the node (weighted averaging). The contributions of the pulses from this area are weighted by a Hamming function which takes the following form:

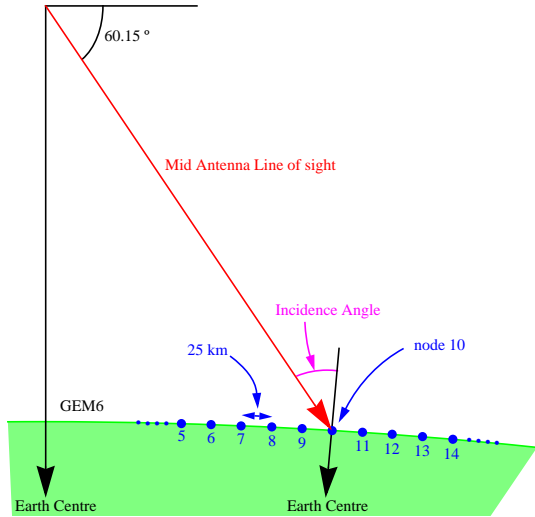


Figure 23: Definition of the node localisation

$$w(n) = \alpha + (1 - \alpha) \cos\left(\frac{2\pi}{N}n\right) \quad \text{eq: 1}$$

where,

$$|n| = \frac{N}{2} \quad \text{eq: 2}$$

The main concept of the spatial filtering are shown on Fig. 24.

By using trigonometric relations it can be shown that this equation is a cosine squared function which sits on a pedestal above the zero level. In general the Hamming window is designed to have a Fourier transform with low sidelobes. The value of α (which can vary between 0 and 1) used in the scatterometer weighting function is set to 0.54. This value produces the optimum level of sidelobe

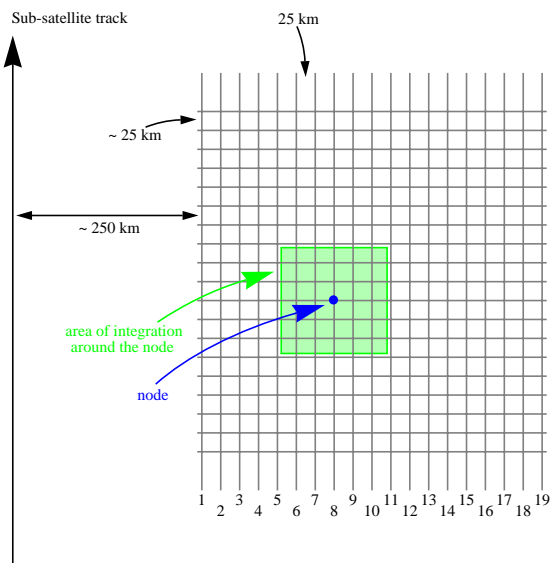


Figure 24: Node localisation

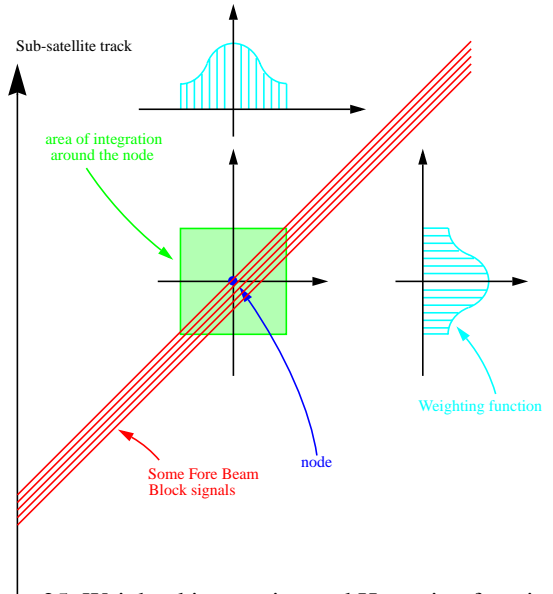


Figure 25: Weighted integration and Hamming function

suppression, such that the highest sidelobe is -43 dB below the peak value.

The Hamming function used in the spatial averaging process will dominate the form of the scatterometer impulse response function. The special properties of this function are important when considering whether the scatterometer data can be regarded as being adequately or inadequately sampled.

The size of the Hamming function is 84.5 km by 84.5 km across and along track respectively for the Side antennae, and 86.0 km by 86.0 km for the Mid antenna.

This part of the processing impact a lot the characteristics of the σ^o and in particular the resolution.

Kp Calculation

In order to allow an optimised wind field extraction algorithm, each σ^o value has to be characterised by the accuracy to which it has been measured. taking into account speckle and receiver noise contributions only and assuming that the noise subtraction process gives only a negligible contribution (noise signal integration time is comparable with the target signal integration time, which is true for ERS), the standard deviation Kp of the σ^o can be written as:

$$Kp = \frac{1}{\sqrt{M}} \left(1 + \frac{\sigma_{noise}^o}{\sigma^o} \right) \quad \text{eq: 3}$$

where M is the number of independent σ^o measurements and σ_{noise}^o is the σ^o equivalent of the receiver noise power. As the Kp value is only used as a weighting factor during further processing, a limited accuracy is acceptable for M and σ_{noise}^o .

During this step of the processing M and the noise normalisation factor are extracted from Look-Up-Tables.

Monitoring Parameters

The last steps of the processing consists of the computation of the Power Spectrum characteristics (Centre of Gravity and Standard Deviation), I and Q channels imbalance factors and the Internal Calibration Level. These parameters are provided in the Source Packet Headers for monitoring purpose.

Wind / Wave mode

The algorithms described in the previous paragraphs were proposed between 1985 and 1986, a long time before the actual launch of ERS-1 on July 21, 1991. In parallel to the progress in the design of this processor, the Scatterometer Simulator System was developed. In the context of this note, the main task of the SSS is the generation of the Look-Up-Tables.

At that time the nominal mode for the scatterometer operations was the Wind mode. An experimental mode called the Wind/Wave mode was proposed, but not supposed to be scheduled nominally.

The Wind/Wave mode consists of interrupting the Scatterometer measurements every 200 or 300 km for a time period corresponding to 2 FMA sequences (1 881.68 ms) in order to acquire a small SAR imagette.

Practically ERS-1 was operated in Wind mode only three days during the commissioning phase, and ERS-2 is operated in Wind mode over land only to allow ATSR High Rate data on-board recording (because of the SAR imagettes, the Wind/Wave mode has a relatively high data rate which doesn't allow the ATSR HR operation at the same time). All data over the ocean (excepted the three days in 1991) were acquired with ~2 s interruption every 200 km for Sar imagettes acquisition.

Basically in Wind/Wave mode, two source packets are permanently missing in the Side antennae spatial filter, and are missing half of the time for the Mid Antenna (see Fig. 26 and Fig. 27).

The impact on the σ° is due to a combination of the size of the Hamming function used for the Spatial Filtering which is a bit less than 100 km (see Spatial Filtering) and of the fact that the σ° is not uniform across the averaging area due to the evolution of the incidence angle (the σ° decreases when the incidence angle increases) as illustrated on Fig. 28.

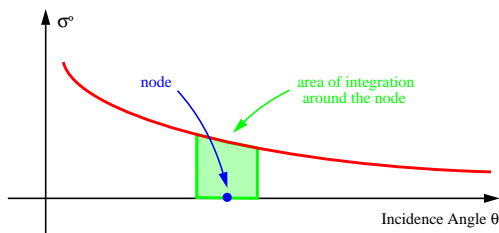


Figure 28: σ° evolution across the swath

If the geophysical phenomena to measured is uniform, the impact on the Mid σ° is negligible as, the same

number of samples are missing inside the integration area at low and at high incidence angle. For the fore and Aft beams the samples are in general not missing in an uniform manner across the node. Fig. 26 shows a situation where high σ° (low incidence angle) samples are missing, therefore the averaged σ° will be slightly lower than what it should have been if all samples were present.

A study was carried out to estimate the impact on the σ° [6]. In case there is no marked structure inside the integration area (well marked meteorological front for example), the error on the Side antennae σ° is lower than

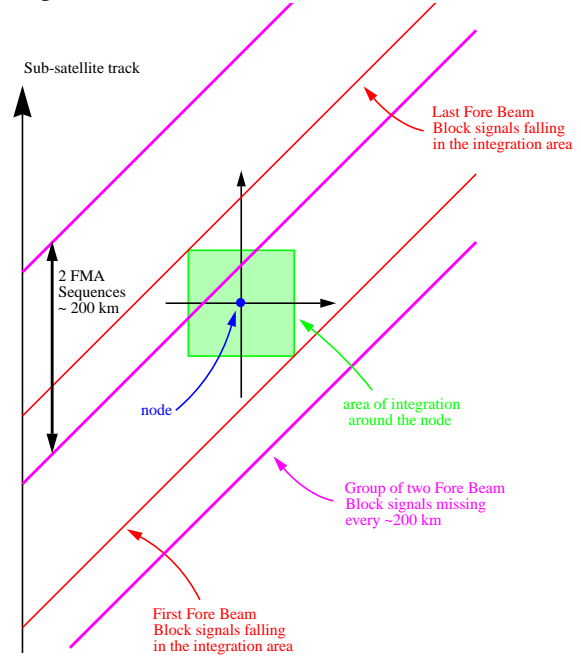


Figure 26: Fore missing Source Packets in Wind/Wave

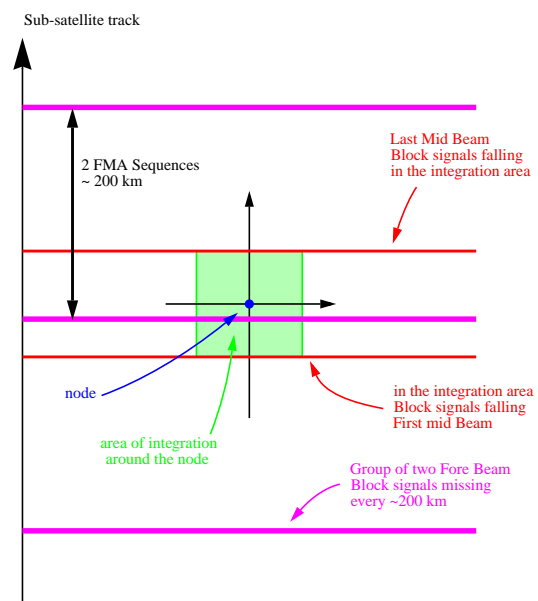


Figure 27: Mid missing Source Packets in Wind/Wave

4% of the nominal σ° value. For the Mid antenna this error is less than 0.1% as expected.

As the normalisation factor are computed in the SSS before hand without knowing the position of the missing source packets, it is impossible to correct this anomaly without modifying completely the actual Ground Processing chains.

σ° to wind processing

This part of the processing chain is the result of various studies carried out by scientific groups in France, United Kingdom and Germany. There are three elements to clearly distinguish. Two are algorithms called Wind Retrieval and Ambiguity Removal and the third element is the model used to relate the σ° and the wind as measured at 10 m altitude. The model used today in the ESA Ground Segment for Real-Time data processing is called CMOD-4 [2]. Very often the quality of the algorithms is confused with the quality of the model when these elements are linked to two different aspects, software engineering on one side, physics of the interaction of the microwave with the sea surface on the other side.

One could propose to use different C-Band models for different type of applications.

It is not the intention to discuss in this document the respective merit of the various existing models; therefore only the algorithms will be presented.

The Wind Retrieval - Principles

This step of the processing is easier to understand when it is represented in the σ° measurement space, defined by the $\sigma^\circ_{\text{fore}}$, $\sigma^\circ_{\text{aft}}$ and $\sigma^\circ_{\text{mid}}$. In this space the C-Band model looks like a double cone as shown on Fig. 29 in an artistic representation and on Fig. 30 as a cut by a plane defined by $\sigma^\circ_{\text{fore}} + \sigma^\circ_{\text{aft}}$ equal a constant value [7].

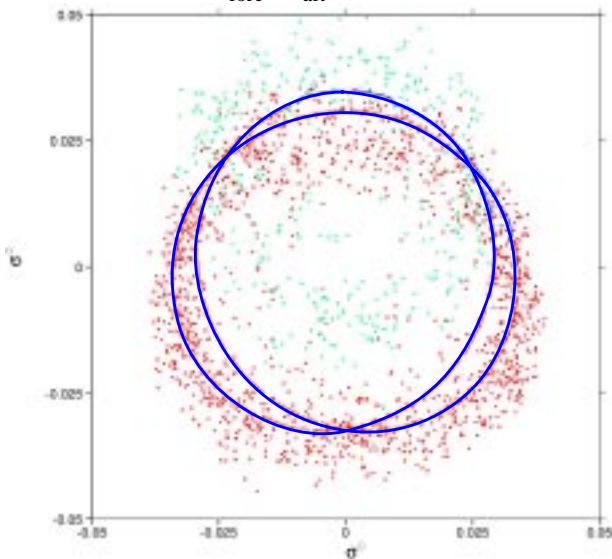


Figure 30: Representation of CMOD 4 (in blue) with ERS-1 and ERS-2 data (respect. in red and in green).

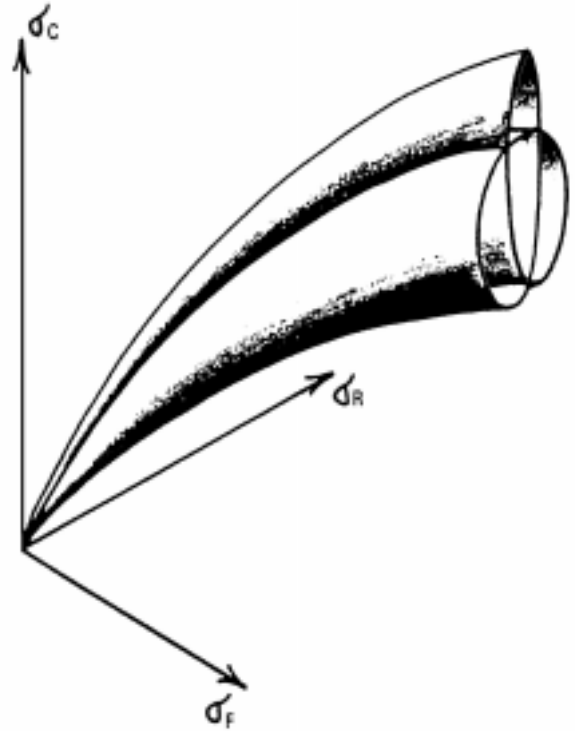


Figure 29: Artistic representation of the C-Band model

This part of the processing consists in finding the minima in the σ° space, of the distance between the σ° triplet measured and this cone.

Historically two definitions of the distance where used.

The first one correspond to the maximum likelihood distance which assumes that each measurement has a gaussian noise of standard deviation kp (see paragraph on kp calculation):

$$M = \sum_{i=1}^3 \left(\frac{\tilde{\sigma}_i - \sigma_i}{kp_i} \right)^2 \quad \text{eq: 4}$$

The second one is simply the Euclidian distance:

$$E^2 = \sum_{i=1}^3 (\tilde{\sigma}_i - \sigma_i)^2 \quad \text{eq: 5}$$

In these equations i is the antenna, $\tilde{\sigma}$ is the measured σ° triplet and σ is the theoretical σ° triplet defined by the C-Band model. The later can be parametrised with the Wind speed v and Wind direction ϕ for a given look angle ψ and the incidence angle θ , these two last variables depending of the antenna.

$$\sigma_i = Model(v, \phi, \psi_i, \theta_i) \quad \text{eq: 6}$$

The model can be internally represented as a Look-Up-Table or an analytical formula. Both representations have been implemented but only the Look-Up-Table was used operationally because of the throughput operational requirement.

The first implementation was based on equation 4, and was giving up to six minima for each σ° triplet. It was latter shown that, because of the non-linearity of the model, the component of the noise parallel and perpendicular to the model were not gaussian, and that there was no real justification for using a maximum likelihood distance.

A new implementation of the wind retrieval algorithm was made based on equation 5. Typically this method returns up to four solutions (see Fig. 31).

The Wind Retrieval - Algorithm Description

The Wind retrieval algorithm is made of four steps:

- Calculation of a realistic Wind Speed as a starting point for the minimisation process.
- Minimisation with a variable wind speed and a fixed wind direction using a Newton-Raphson technique. This minimisation is performed every 10° in wind direction with 0.5 m/s precision if the Look-Up-Table is used and 5° and 0.1 m/s precision if the analytical form of the model is used. 36 (or 72) triplets of speed, direction and distance are calculated. It is important to note that the wind speed retrieved are varying with the wind direction.
- Retrieval of the up to six minima (only four are actually retrieved since the Euclidian Distance method was implemented)
- Ranking of the minima from the smallest distance to the largest (Rank 1 to 6).

When the C-Band model is modified, the convergence of the Newton-Raphson minimisation has to be checked. A tradeoff has to be found between the operational requirements (throughput, memory and processing power available) and the size of the Look-Up-Table. When this algorithm was installed for ERS-1, the best trade-off was 10° and 0.5 m/s resolution, these specifications were never changed even if the hardware was

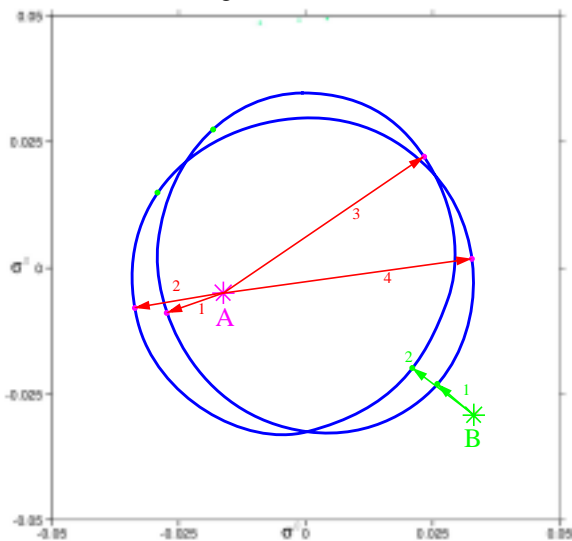


Figure 31: Illustration of an example of wind solutions retrieval (A and B have respectively 4 and 2 solutions)

upgraded twice (once just before ERS-1 launch and a second time just before ERS-2 launch).

The output of this part of the processing are the up to four solutions (wind speed and direction) and the distance from the solution to the cone.

The Ambiguity Removal

The ambiguity removal consists in choosing the right solution within the up to four computed by the Wind retrieval.

The capacity of choosing the right solution in an autonomous way (i.e. without any external support from analysis or forecasts) depends directly on the relative distance between the two sheets of the cone and the measurement noise. In another words, if the noise doesn't "move" the measurement point from the cone further than half the distance between the two sheets, the rank one solution is most of the time the correct one.

This is not the case. If fact Fig. 30 indicates that the noise and the distance between the two sheets are of the same order of magnitude. The quality of the C-Band model is also very important. Errors in the model description will lead directly to errors in the distances and eventually to the wrong solution.

Pratically the algorithm implemented uses two methods, an autonomous one which works only in certains conditions (high uniform winds with a direction which corresponds to an area of the cone where the two sheets are well separated) and a second method which uses the support of forecasts produced by ECMWF.

Due to operational reasons (generation and transmission time), the forecasts used are 18, 24, 30 and 36 hours forecasts valid for ambiguity removal for a period of 6 hours from -3 to +3 hours around the nominal time. This will be improve soon, as ECMWF produces these forecast twice a day (and not only once as before). Starting in October 1998 only 18 and 24 hours forecasts are used twice a day.

In both cases the algorithm uses a statistical approach. Based on the first two solution for each node (rank 1 and 2) two coherent wind fields are constructed, where each node in one of the field is 180° appart of the same node in the other field ("opposite" wind fields). By counting the number of rank 1 solution in each field (autonomous method) or by computing an averaged directional distance between each field and the meteorological forecast (meteorological method), the best field is chosen.

In order to optimise the use of the hardware capacity and to avoid to propagate ambiguity removal errors, it has been decided to work on continuous segment of the swath up to 3000 km (6 products) long.

New ambiguity removal methods using in particular 2 dimensional variational techniques are being studied and made available. The possibility of implementing such a technique is being investigated.

The Ambiguity Removal - Algorithm Description

Five main steps are presents in both methods.

- Select six consecutive products
- Define continuous zones within the selected 6 products (these zones are interrupted by land, no wind area)
- Using rank 1 and rank 2 solutions build two “opposite” wind fields for each of the zones. The algorithm in place works by continuity, choosing the solution which has a direction close to the previous two nodes.
- Select by using the autonomous and/or the meteorological method the “best” wind field.
- Introduce rank 3 and 4 solution by cheking if they make the retrieve wind field smoother.

Conclusion

References

- [1] E. Attema, “The Active Microwave Instrument On-Board the ERS-1 Satellite”, Proc. IEEE, Vol. 79, No 6, pp. 791-799, June 1991.
- [2] Lecomte P., “CMOD4 Model Description”, ESA technical note, issue 1.2, March 1993.
- [3] T.D. Guyenne, “Engineering Achievement of ERS-1”, ESA SP-1176/III, October 1997.
- [4] Pulliainen J., J. Grandell, M. Hallikainen, M. Virtanen, N. Walker, S. Metsaemaeki, J.P. Ikonen, Y. Sucksdorff, T. Manninen, “Scatterometer and Radiometer Land Applications”, ESRIN Contract: 11122/94/I-HGE(SC), 253 p., April 1996
- [5] Cavanié A., P. Lecomte, “Study of a method to dealise winds from ERS-1 data”, ESA contract 6874/87/GP-I(sc), 1987.
- [6] Wuttge S., H. Munz, “Effect of Gaps in Scatterometer Raw Data on σ^0 -Triplets”, ER-TN-DSF-FL-0001, May 1995.
- [7] Cavanie A., J. Demurger and P. Lecomte, “Evaluation of the different parameters in Long’s C-band model” Proceedings of a Workshop on ERS-1 Wind and Wave Calibration, Schliersee, FRG, 2-6 June, 1986 (ESA SP-262, Sept. 1986), pp 47-51.
- [8] Long A.E., “Toward a C-Band Radar Sea Echo model for the ERS-1 Scatterometer”, Proc. of the Third international Colloquium on Spectral Signa-

ture of Objects in Remote Sensing, les Arcs 1985, (ESA SP-247).

- [9] Long A.E., “ERS-1 C-Band and Sea-Echo Models”, ESA internal Report ESTEC/WMA/9104, Rev. 1. April 1991.
 - [10]Offiler D., “Validation of ERS-1 Scatterometer Winds; An appraisal of Operational Backscatter Model Performances from launch to Present”, NOAA/NESDIS Workshop Proceedings, Alexandria, VA, USA, April 1996.
 - [11]Stoffelen, A.; “Improvement and Quality Assurance of the scatterometer Wind Product in the Backscatter Domain.” Proceedings of the CEOS Wind and Wave Validation Workshop, ESA WPP-147, 159-160, 1997.
 - [12]Stoffelen, A., D. Anderson, “Characterisation of ERS-1 Scatterometer measurements and wind retrieval.” Proc. of the Second ERS-1 Symposium - Space at the service of our environment, Hambourg 1993, ESTEC, Noordwijk. The Netherlands, (ISBN 92-9092-286-9).
- ## Other various References
- [13]Attema E. “Estimating Satellite Pointing Biases from Scatterometer transponders Measurements - An exact Solution”, ORM/3078/EA/sml, 14 March 1989.
 - [14]Attema E., “The Design, Calibration and System Performances of the ERS-1 and ERS-2 Wind Scatterometer”, NOAA/NESDIS Workshop Proceedings, April 1996, Alexandria, VA, USA.
 - [15]Graham R. et Al., “Evaluation of ERS-1 Wind Extraction and Ambiguity Removal Algorithms”, ESA Contract, January 1989.
 - [16]Guyenne D. ed., “ERS-1 A new tool for global environmental monitoring in the 1990’s”, ESA BR-36, November 1989, ESTEC, Noordwijk. The Netherlands, (ISBN 92-9092-019-X).
 - [17]Lecomte P. et Al., “ERS product Assurance and Quality Control”, ESA Bulletin 82, May 1995, ESTEC, Noordwijk, The Netherlands, (ISSN) 0376-4265).
 - [18]Lecomte P., Attema E.P.W., “Calibration and Validation of the ERS-1 Wind Scatterometer”, Proc. First ERS-1Symposium,4-6November1992,Cannes,France.

- [19] Longdon N. ed., "ERS-1 Data Book", ESA BR-75, April 1991, ESTEC, Noordwijk. The Netherlands, (ISSN 0250-1589).
- [20] Mestre O., "Réponse du diffusiomètre d'ERS-1 en fonction de l'angle d'incidence", note de travail de L'ENM 462, 1993.
- [21] Vass P., B. Battrick ed., "ERS-1 System", ESA SP-1146, September 1992, ESTEC, Noordwijk. The Netherlands, (ISSN 0379-6566).
- [22] Wooding M. ed., "ERS-1 Geophysical Validation, Workshop Proc.", ESA WPP-36, August 1992, ESTEC, Noordwijk. The Netherlands.

Documentation

This paper was written using intensively internal documentation released by industry during the ERS Active Microwave Instrument development on one side and during the various studies in preparation for the ground processing and for its development on the other side. This documentation cannot be made available to external users.

- [I-1] ERS-2 Satellite to ground Segment Interface Specification - ER-IS-ESA-GS-0002 - Issue 1.1, 02.12.1993
- [I-2] Kiruna Station Requirements Specification - ER-RS-DSF-GS-0002
- [I-3] ERS-2 AMI Flight model Characterisation Data - ER-TN-ESA-GS-0447 - Issue 1.0, 17.03.1995
- [I-4] Wind Scatterometer Ground Processing Requirements up to σ^0 - ER-RP-DSF-SY-0006 - Issue 4, 18.12.1987, hand write updated June 1990.